Electronic Supplementary Information for

Efficient CO_2 Conversion by Biocompatible N-doped Carbon Nanosheets coupled with *Ralstonia eutropha*: Synergistic Interactions between Microbial and Inorganic Catalysts

Jiani Yao, [a] Youzhi Li, [b] Siyuan Xiu, [a] Shujie Zheng, [c] Ying Huang, [c] Zijing Zhou, [d] Yang Hou, [a] Bin Yang, [a,b] Lecheng Lei, [a,b] Zhongjian Li *[a,b]

a. Key Laboratory of Biomass Chemical Engineering of Ministry of Education, College of Chemical and Biological Engineering, Zhejiang University, Hangzhou 310027, China

b. Institute of Zhejiang University - Quzhou, Quzhou, 324000, China

c. School of Environment, Hangzhou Institute for Advanced Study, University of Chinese Academy of Sciences, Hangzhou 310024, China

d. Zanvyl Krieger School of Arts & Sciences, Johns Hopkins University, Baltimore, MD 21218, USA

Table of contents

Text 1 Electrode Fabrication and Characterization

NC. NC precursor was synthesized by mixing a given mass ratio of NH_4Cl (Sigma-Aldrich, AR) and Ethylene Diamine Tetraacetic Acid (EDTA, Sigma-Aldrich, AR) into 250 mL deionized water under intensely stirring for 1h at 60°C, the solution was concentrated by rotary evaporation and then dried at 60°C for 12 h. The ground mixture was then annealed under an argon atmosphere at a heating rate of 10°C min^{-1} for 2 h at 1000°C. The mass ratios of NH_4Cl and EDTA were selected as 8:1, 4:1, 1:and 1, 0 (only EDTA). The precursor with a mass ratio of NH_4Cl to EDTA of 8:1 was additionally carbonized at 900 and 800°C. The obtained products were named as NC-8-1000, NC-4-1000, NC-1-1000, NC-EDTA-1000, NC-8-900 and NC-8-800, respectively.

NiMoZn. The NiMoZn cathodes were prepared by electrodepositing onto 304 stainless steel mesh using a previously reported procedure.1 The electrolyte consisted of $NiCl_2$•$6H_2O$ (9.51 g L^{-1}), Na_2MoO_4•$2H_2O$ (4.84 g L^{-1}), $ZnCl_2$ (0.0409 g L^{-1}), $Na_4P_2O_7$ (34.57 g L^{-1}) and $NaHCO_3$ (74.77 g L^{-1}). Hydrazine hydrate (1.21 mL L–1; Alfa Aesar) was added immediately before plating. After pre-treatment at –2 V vs. Ag/AgCl in 0.5 M H_2SO_4 for 3 min, the stainless steel was plated at a current density of 0.0775 A cm^{-2} for 30 min. The NiMoZn was obtained after leaching for 24 h in 10 M KOH.[1]

Electrochemical measurements. The linear sweep voltammetry (LSV), electrochemical impedance spectroscopy (EIS), and, cyclic voltammetry (CV) were performed using a versatile electrochemical workstation (VSP300, BioLogic, France) with a typical three-electrode cell. A graphite rod was used as a counter electrode and Ag/AgCl electrode a as reference electrode. The working electrode was prepared by following procedure: the NC catalyst (10mg) was dispersed in 900 μL of ethanol and 100 μL of 0.5 wt.% Nafion. The dispersed solution was sonicated for 1h and stirred for 12h, and then catalyst ink was drop-coated onto a 3 mm glassy carbon electrode (loading concentration ~0.28 mg cm^{-1}) or 2 cm x 2 cm carbon paper (loading concentration ~1 mg cm^{-1}determineimined the HER performance of NC-8-1000 coupled with wild-type *R. eutropha* H16 or C5ΔMBHΔSH, the corresponding bacteria were cultured to OD_{600} = 2.0 and 50 mL of bacterial suspension was concentrated to 5ml, and then 2 μL concentrated bacterial suspension was dropped on glassy carbon loaded with NC-8-1000. In the optimization experiment, glassy carbon loaded with catalysts was used as a working electrode for LSV tests while carbon paper loaded with catalysts was used for CV, EIS, and LSV in the comparison experiment with NiMoZn. The LSV was recorded at a scan rate of 5mV s^{-1} and EIS was examined over a frequency range of 0.1 MHz − 0.01 Hz. All currents were corrected by an 80% iR compensation. Since the electrochemical active surface area (ECSA) is proportional to the double-layer capacitances (C_{dl}), it can be estimated by calculating $C_{dl,}$ which was acquired by CV in 1M PBS at scan rates from 10 to 50 mV s^{-1} in the non-Faradaic region (0.2 to 0.3 V vs. RHE). The C_{dl} was calculated by plotting the ja-jc at 0.25 V (where jc and ja are the cathodic and anodic current density, respectively) vs. RHE against the scan rate, where the slope was twice that of C_{dl}.

The RRDE curves were collected using a glassy carbon disk electrode surrounded by a Pt ring (4 mm inside diameter). The electron transfer number (n) and the corresponding peroxide species (HO^{2-}) were calculated with the equation (1) and (2),

$$n = \frac{4I_{disk}}{I_{disk} + I_{ring}/N} \quad (1)$$

$$HO^{2-}\ (\%) = \frac{200 I_{ring}/N}{I_{disk} + I_{ring}/N} \quad (2)$$

where I_{disk} and I_{ring} are the disk electrode current and ring electrode current (A), respectively. The Pt ring electrode was polarized at 0.5 V (vs Ag/AgCl), and N is the collection efficiency of the ring electrode (N = 0.42).

Materials characterization. Morphological properties were examined using scanning electron microscopy (SEM, Hitachi SU-8010, Japan) and high-resolution transmission electron microscopy (HR-TEM, JEOL, JEM-2100F, Japan). Elemental distributions were assessed by energy dispersive spectroscopy (EDS) using the same SEM and HR-TEM. Surface chemical compositions were analyzed by high resolution X-ray photoelectron spectroscopy (HR-XPS, ThermoFisher 250XI, USA) and X-ray diffraction (XRD, Shimadzu XRD-6000, Japan). Raman spectra were recorded on a Raman microscope (Horiba Jobin Yvon, LabRAM HR Evolution, France) under an excitation laser of 532 nm. The specific surface areas were measured using a surface area analyzer (Micromeritics, ASAP 2460, USA) based on the N_2 physisorption test, and calculated by the Brunauer–Emmett–Teller (BET) method. The pore size distributions were calculated from their N_2 physisorption isotherms using the non-local density functional theory (NL-DFT) method. The water contact angles were measured with a contact angle measuring device (OCA 20, Data Physics Instruments GmbH). The surface functional groups were identified by a Fourier transformation infrared spectrometer coupled with an infrared microscope (FT-IR, EQUINOX 55). The biofilm growth and cell viability were examined using a confocal laser scanning microscopy (CLSM, Olympus FV1200, Japan) with a LIVE/DEAD assay kit (the green/red fluorescence refers to the live/dead cells).

Text 2 Hybrid System Construction

Bacterial cultivation. *Ralstonia eutropha* H16 (ATCC=17699) was purchased from BeNa Culture Collection. C5ΔMBHΔSH was obtained from Jiazhang Lian's group at Zhejiang University. *R. eutropha* H16 was successively precultured in broth medium and minimal medium with 10 g L^{-1} D-fructose at 30°C for 12 h. 20 mL pre-culture were centrifuged at 7000 rpm for 7 min, and then washed twice and resuspended in 5 mL of minimal medium for subsequent inoculation into the reactors. The minimal medium was composed of Na_2HPO_4•$7H_2O$ (18 g L^{-1}), KH_2PO_4 (3 g/L), $(NH_4)_2SO_4$ (0.2 g/L), $MgSO_4$•$7H_2O$ (0.15 g L^{-1}), $NaHCO_3$ (0.3 g L^{-1}), ferric citrate (0.05 g L^{-1}), $CaSO_4$•$2H_2O$ (1 mg L^{-1}), $NiSO_4$•$7H_2O$ (0.56 mg L^{-1}), trace element solution (1 mL L^{-1}) and gentamicin (10 mg L^{-1}). The trace element solution contained (1 L): 1.5 g NTA, 0.3 g H_3BO_3, 0.2 g $CoCl_2$·6 H_2O, 0.1 g $ZnSO_4$·7 H_2O, 0.03 g $MnCl_2$·4 H_2O, 0.03 g Na_2MoO_4·2 H_2O, 0.02 g $NiCl_2$·6 H_2O, and 0.01 g $CuSO_4$·5 H_2O. All mediums were sterilized by autoclaving for 30 min, except fructose and gentamicin which were filtered through a sterile filter. The minimal medium was also used as an electrolyte in the bioelectrochemical reactors.

Gene knockout and construction of C5ΔMBHΔSH.

Suicide plasmid pK19mobSacb and two homologous templates with a length of 500 bp were applied for gene knockout. The knockout plasmids were constructed by the Gibson method and then introduced into E. coli S17 by conjugation. The recombinant strains were screened as follows: the single clones on LB plates were verified by colony PCR, and then the suicide plasmids-bearing bacteria were cultured in LB with 100 g L^{-1} sucrose but without NaCl at 30 °C for 72 h. After 72h, the bacteria solution was diluted 1000 times was cultured on an LB plate at 30 °C for 48 h. Several single clones were selected and cultured in LB with and without kanamycin at 30 °C for 24 h respectively. Then the recombinant strain was verified by PCR amplification. Because membrane-bound hydrogenase (MBH) is harder to knock out than soluble hydrogenase (SH) genes, SH was knocked out based on C5ΔMBH, and a hydrogenase-deficient strain C5ΔMBHΔSH was constructed.

Reactors. All experiments were conducted in single enclosed chamber reactors with a working volume of 150 mL at 30°C. The reported data are based on at least three biological replicates ($n \geq 3$). A carbon paper (2 × 2 cm^2) coated with NC (1mg cm^{-2}) or NiMoZn (2 × 2 cm^2) served as the cathode for HER, while a platinum net was used as an anode for OER. Each reactor contained a 1.5 cm stirring bar rotating at 500 rpm. The reactors after sterilization were filled with 150 mL of minimal medium and then purged with pure CO_2 for 30 min. Subsequently, the resuspended *R. eutropha* H16 was transferred into reactors (initial OD_{600} = 0.2 in the general experiment). The cycles ended when the OD decreased significantly, no more than 10 days. In a long-term experiment, the minimal medium was completely renewed at the end of each cycle and *R. eutropha* H16 was reinoculated at the beginning of cycle 2,4,6 until the initial OD_{600} reached ~ 0.5. To explore the effect of applied current on the bioelectric conversion of CO_2, the current density of 4.5, 6, 9 mA cm^2 were applied in cycle 1-2, 3-4, 5-6, respectively. All reactors were operated continuously for 24 h, followed by sampling and CO_2 purging. 2 mL of solution was sampled from each reactor and centrifuged at 7000 rpm for 7 min after detection of OD_{600}. The supernatant was used for the detection of metal leaching and the sediment was cryopreserved for subsequent quantification of PHB. The OD_{600} was measured by a UV-visible light spectrophotometer (Thermo Scientific Evolution 201, USA) at 600nm. The reactors were galvanostatically controlled by a versatile electrochemical workstation (VSP300, BioLogic, France).

Text 3 Analysis and Assays

Toxicant quantification. Both H_2O_2 and •OH concentrations were monitored by fluorometric analysis using a microplate reader (infinite 200Pro, TECAN, Switzerland). Specifically, H_2O_2 concentration was assayed using an Amplex Red H_2O_2 detection kit (Sigma-Aldrich) with λ_{ex} = 540 nm and λ_{em} = 590 nm. The •OH concentration was monitored by fluorimetric analysis (λ_{ex} = 320 nm, λ_{em} = 425 nm) of the 2-hydroxyterephthalic acid formed by the reaction of •OH with terephthalic acid. The concentration of leached metals in the electrodes was measured with an inductively coupled plasma optical emission spectrometer (ICP-OES, Thermo Scientific ICAP Pro X, USA).

A 10 μL culture was diluted 1:100 in the fresh minimal medium for spotting. Four serial 10-fold dilutions of this sample were made, with 2 μL of each was spotted on broth-rich agar plates and allowed to dry on the benchtop. Plates were typically grown at 30 °C for 6 h before imaging.

The quantification of PHB. The amount of poly-β-hydroxybutyrate (PHB) was analyzed by high-performance liquid chromatography (HPLC, Agilent HPLC 1260, USA) equipped with an Aminex HPX-87H column. Before the HPLC analysis, the sediment of centrifuged samples was digested with 98 wt.% H_2SO_4 at 90°C for 60 min. The digested solution was diluted with DI water and passed through a 0.22 μm filter. Samples were analyzed under the following conditions: mobile phase, 2.5mM H_2SO_4 aqueous solution; flow rate, 0.5 mL/min; injection volume, 100 μL; column temperature, 30°C; detection at 210 nm. The interval between two injections was 40 min.

Efficiency calculation. The efficiency values reported in this work were calculated based on previous work.[2] To calculate energy efficiency, the following parameters need to be obtained first,

$$OD_{biomass} = OD_{600} - \frac{c_{PHB}}{831} \quad (3)$$

$$c_{biomass} = 448 \times OD_{biomass} \quad (4)$$

$$DCW = c_{biomass} + c_{PHB} \quad (5)$$

where $OD_{biomass}$ excluding the light scattering from PHB accumulation, $c_{biomass}$ and c_{PHB} were the concentration of biomass and PHB converted from CO_2 (mg L^{-1}), DCW was the dry cell weight (mg L^{-1}).

The electricity conversion efficiency (EE) was defined as follows,

$$EE = \frac{\sum n \times \Delta_r G^0}{I \times U \times t} \quad (5)$$

where I was the current applied on the reactor (A), U was the voltage monitored between the cathode and anode (V), and t was the duration of the reaction (s). n was the amount of organic converted from CO_2 (mol). $\Delta_r G^0$ was the Gibbs free energy gaining from CO_2 to organic (including biomass and PHB) (J mol^{-1}). $\Delta_r G^0$ for specific target products, along with the corresponding chemical reactions, are listed in the following,

Biomass formation:

$CO_2(g) + 0.24\ NH_3(aq) + 0.525\ H_2O\ (\ell) \rightarrow CH_{1.77}O_{0.49}N_{0.24}(s) + 1.02\ O_2(g)$

$\Delta_r G^o$ = 479 kJ/mol

PHB formation:

4n $CO_2(g)$ + 3n $H_2O(\ell)$ → $(C_4H_6O_2)_n(s)$ + 4.5n $O_2(g)$

$\Delta_r G^o \sim \Delta_r H^o$ = 1903 kJ/mol per monomer

DFT Calculation method. The present first principle DFT calculations are performed by Vienna Ab initio Simulation Package(VASP)[3] with the projector augmented wave (PAW) method[4]. The exchange-functional is treated using the generalized gradient approximation (GGA) of the Perdew-Burke-Ernzerhof (PBE) functional.[5] All calculations were performed with Spin-polarizations. The energy cutoff for the plane wave basis expansion was set to 520 eV, and the force on each atom less than 0.03 eV/Å was set as the convergence criterion of geometry relaxation. The k-points in the Brillouin zone were sampled by a 3 × 3 × 1 grid. A convergence energy threshold of 10^{-5} eV was used for the self-consistent calculations. The DFT-D3 method was employed to consider the van der Waals interaction.[6] The computational model was constructed based on a 5×5 supercell on the surface of a single layer of graphene (001) (containing 50 atoms). To avoid interactions between periodic structures, a vacuum of 15 Å was added along the z direction.

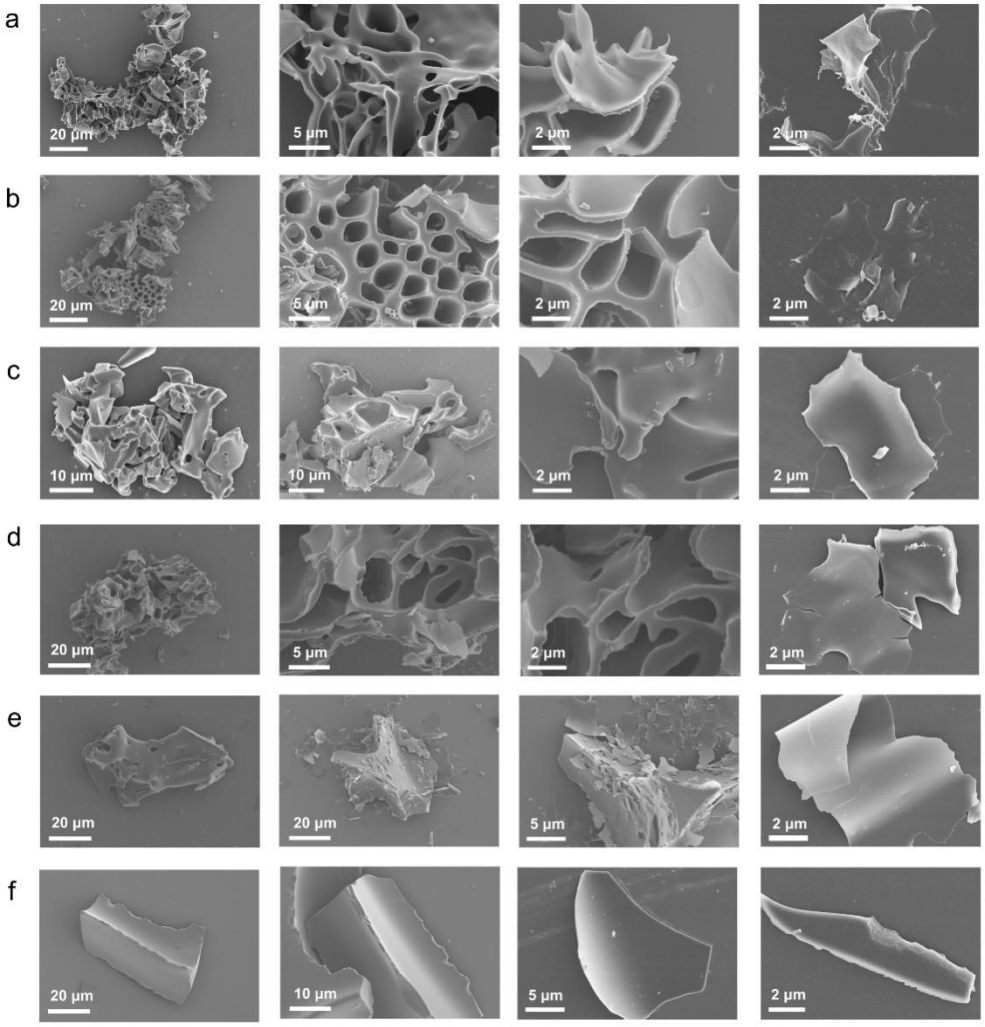

Figure S1 SEM images of a) NC-8-1000, b) NC-8-900, c) NC-8-800, d) NC-4-1000, e) NC-1-1000, and f) NC-EDTA-1000

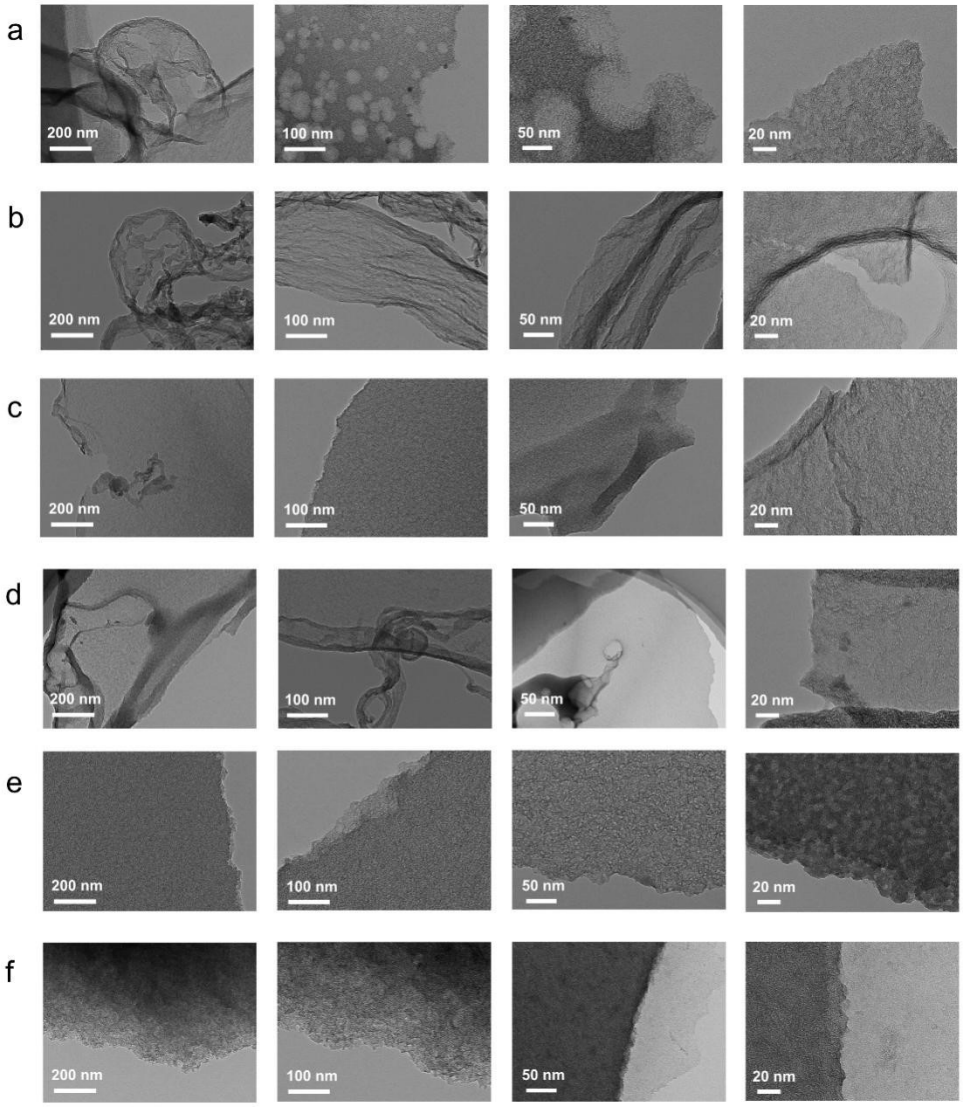

Figure S2 TEM images of a) NC-8-1000, b) NC-8-900, c) NC-8-800, d) NC-4-1000, e) NC-1-1000, and f) NC-EDTA-1000

To investigate the evolution process of NC, a series of conditional experiments on carbonization temperature and precursor mass ratio were carried out. As shown in the Scanning/transmission electron microscopy (SEM/TEM) images (Fig. S1 and S2), after carbonizing the precursors at a relatively low temperature of 800 °C, three-dimensional porous carbon blocks and scattered few flakes (NC-8-800) can be observed. When the carbonization temperature rose to 1000 °C, a three-dimensional porous carbon network with ultrathin nanosheets was formed (NC-8-1000). Comparing the obtained products with different precursor mass ratios, the NC nanosheets became progressively thinner and showed more convolutions and pores as the NH_4Cl in the precursor increased, while only large carbon blocks (NC-EDTA-1000) could be foamed without the presence of NH_4Cl. It is attributed to more NH_4Cl as a gas-foaming agent, triggering a more vigorous blowing action in the carbonization process at 1000 °C.

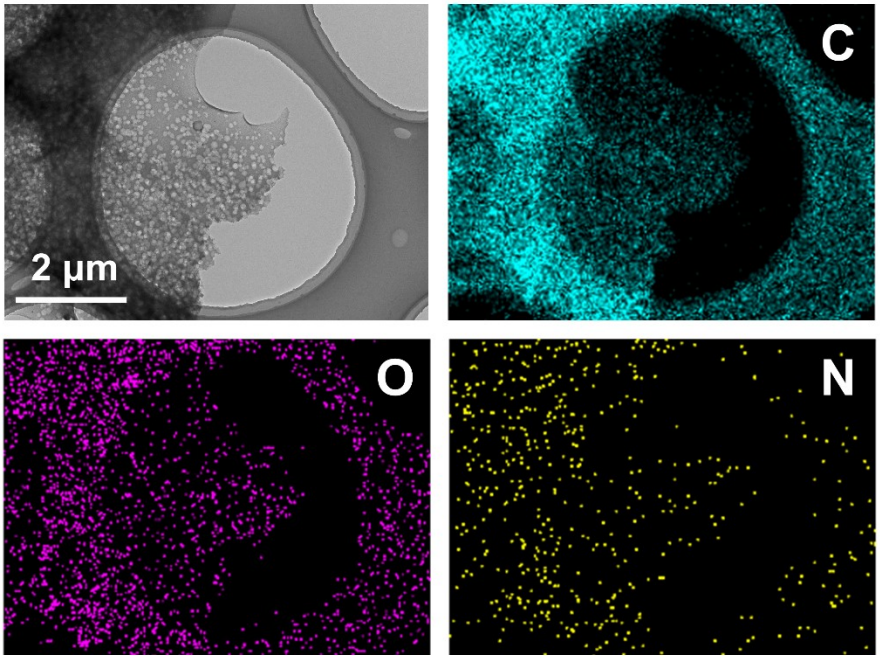

Figure S3 STEM image of NC-8-1000 and the corresponding elemental mapping images of C, O, and N elements.

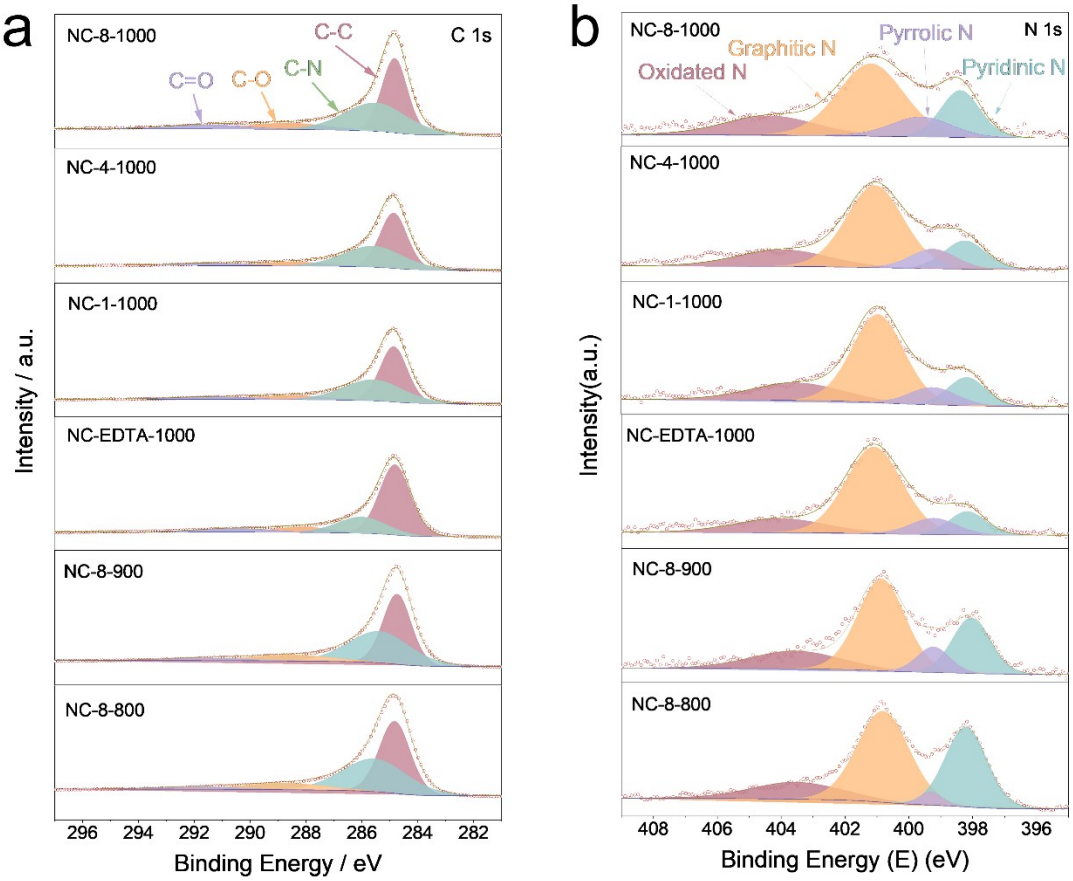

Figure S4 The high-resolution a) C 1s and b) N 1s XPS spectra of NC-8-1000, NC-8-900, NC-8-800, NC-4-1000, NC-1-1000, and NC-EDTA-1000.

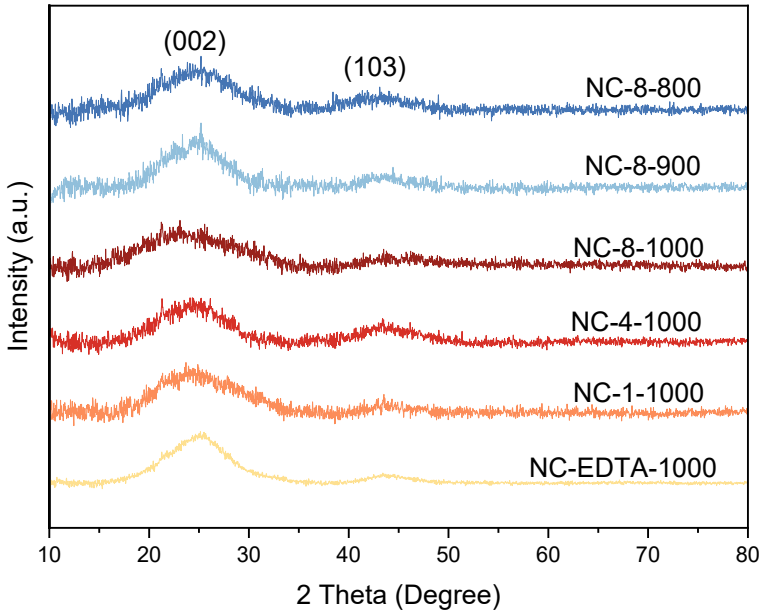

Figure S5 XRD patterns of NC-8-1000, NC-8-900, NC-8-800, NC-4-1000, NC-1-1000, and NC-EDTA-1000.

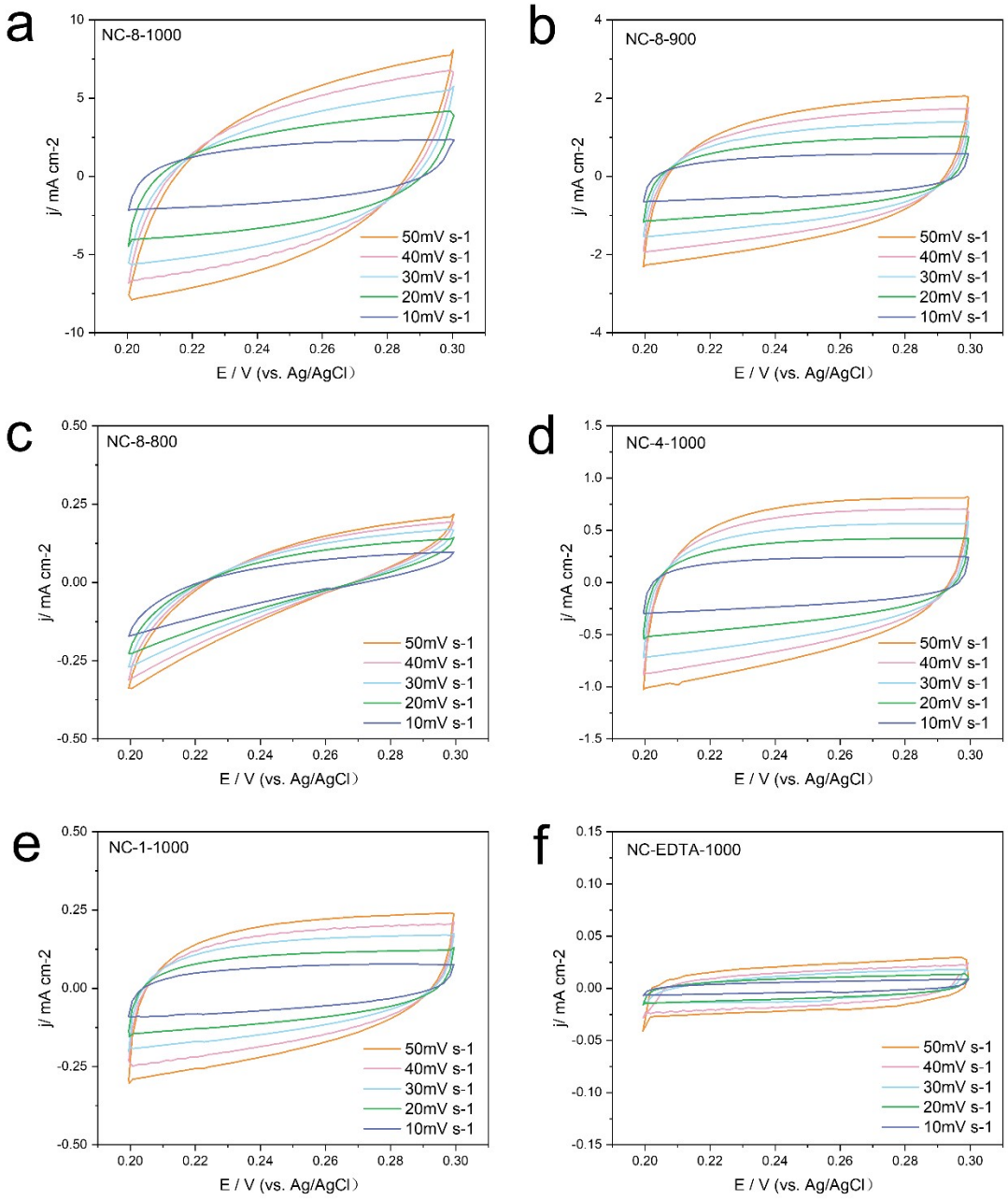

Figure S6 CV curves of a) NC-8-1000, b) NC-8-900, c) NC-8-800, d) NC-4-1000, e) NC-1-1000, and f) NC-EDTA-1000 with different scanning rates of 10, 20, 30, 40, and 50 mV s^{-1} for the ECSA calculation.

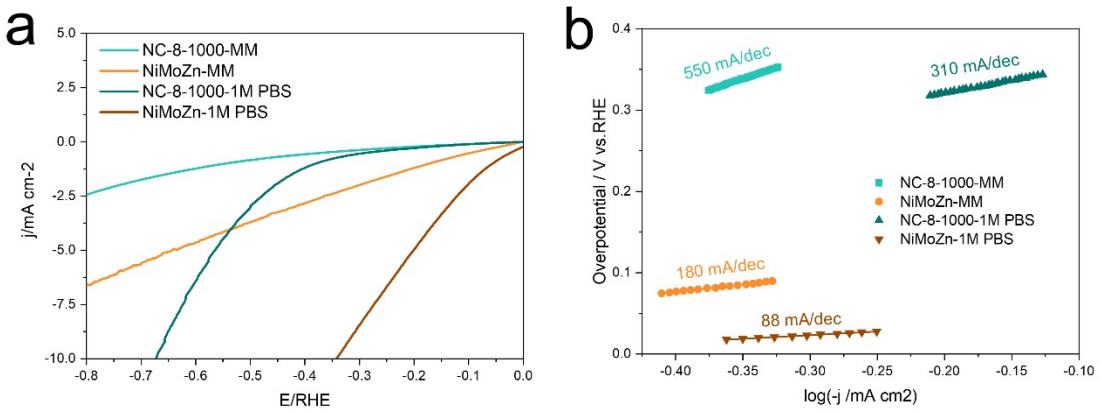

Figure S7 a) LSV curves and b) Tafel plots of NC-8-1000 and NiMoZn in MM and 1 M PBS.

The catalytic activity of NiMoZn (onset potential – 0.019 V vs. RHE and Tafel slope 94 mV dec^{-1}) was much higher than NC-8-1000 in 1M PBS due to the high conductivity and electron-rich properties of metal catalysts. Nevertheless, the catalytic activity of both NC-8-1000 and NiMoZn decreased significantly in MM. It is not surprising that the performance of inorganic catalysts is inhibited in the biological medium due to the low conductivity (8.8 mS cm^{-1} for 1 M PBS, 1.8 mS cm^{-1} for MM) and the existence of complex interfering components (e.g., citric acid).

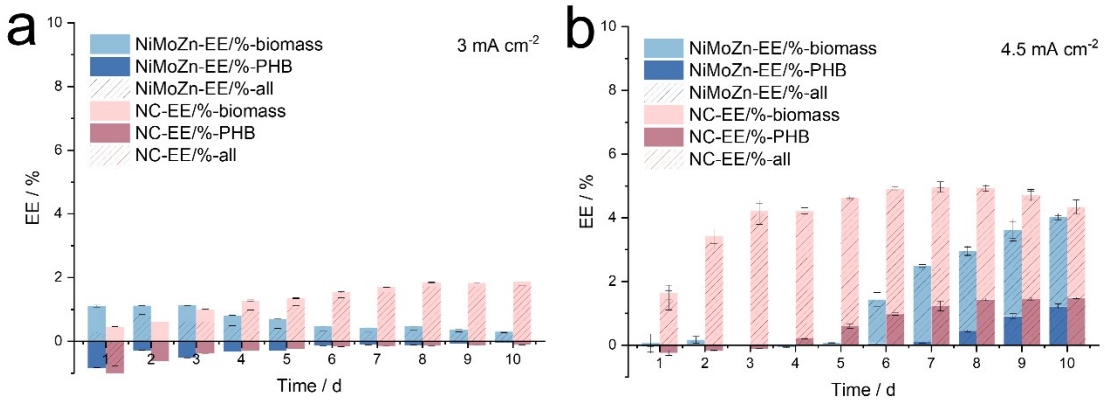

Figure S8 The energy efficiency of converting electrical energy into organic matter, biomass, and PHB in the Pt | NiMoZn and Pt | NC hybrid system applied a) 3 mA cm^{-2} and b) 4.5 mA cm^{-2} current density.

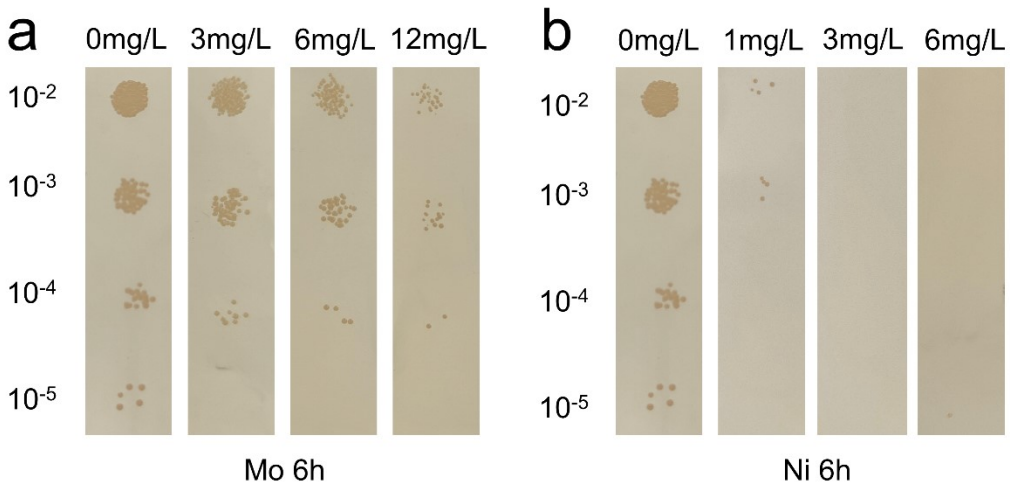

Figure S9 Spot assay of *R. eutropha* H16 for different concentrations of metal ions (MoO_4^{2-} and Ni^{2+}).

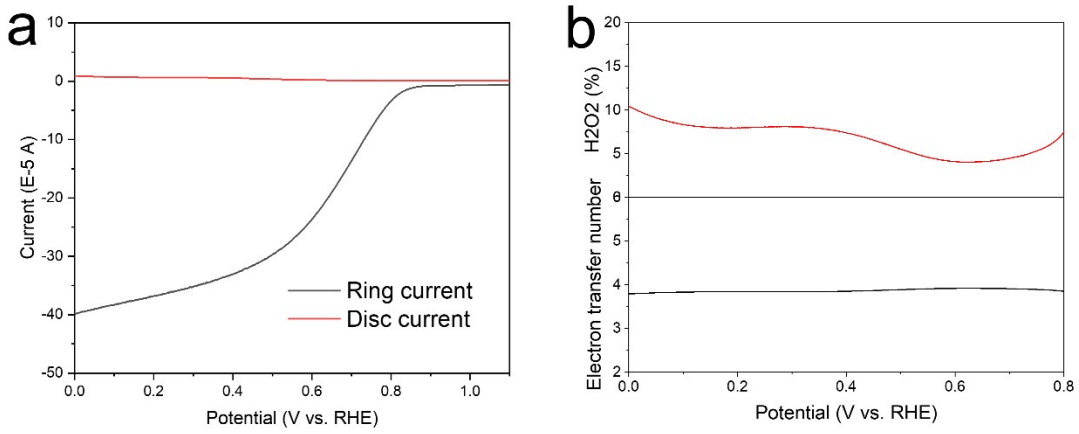

Figure S10 a) RRDE polarization curves at 1600 rpm in O_2-saturated MM solution with a scan rate of 10 mV s^{-1}; b) H_2O_2 selectivity and electron transfer number of NC-8-1000.

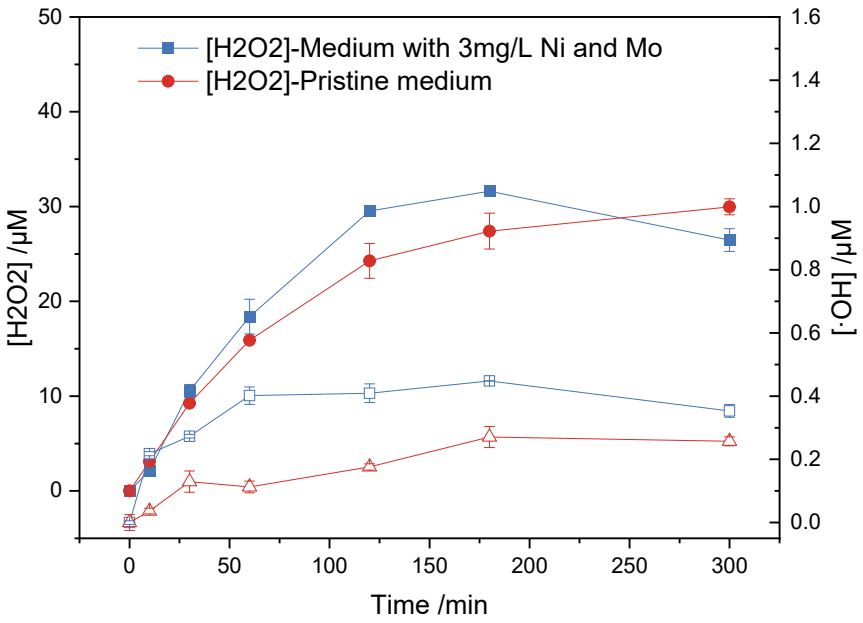

Figure S11 The effect of metal ions (MoO_4^{2-} and Ni^{2+}) on ROS production.

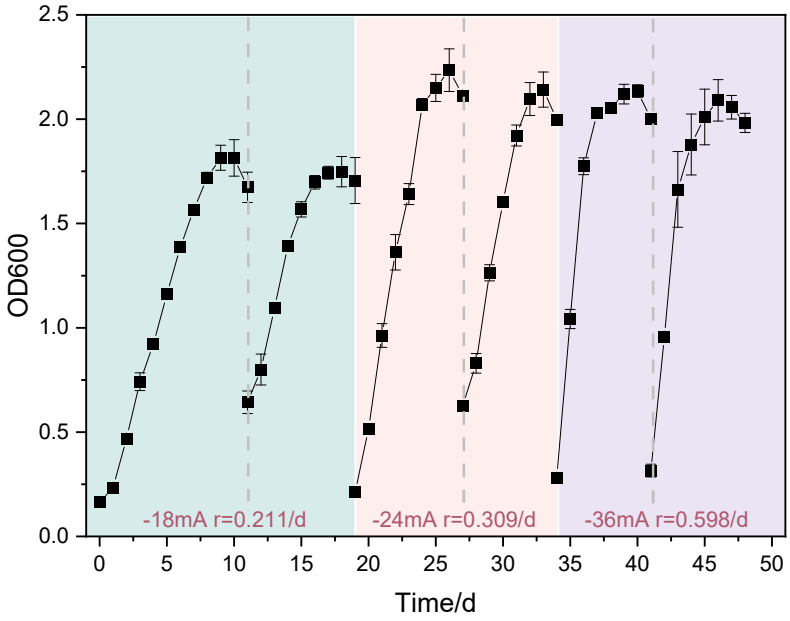

Figure S12 OD_{600} in the long-term experiment.

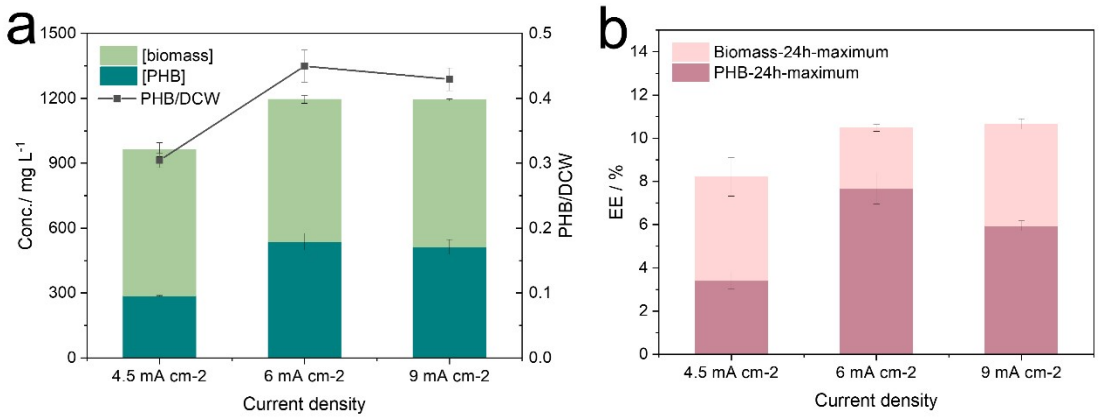

Figure S13 a) maximum yield of biomass and PHB and the content of PHB in DCW b) 24h-maximum energy efficiency at different applied currents in the long-term experiment.

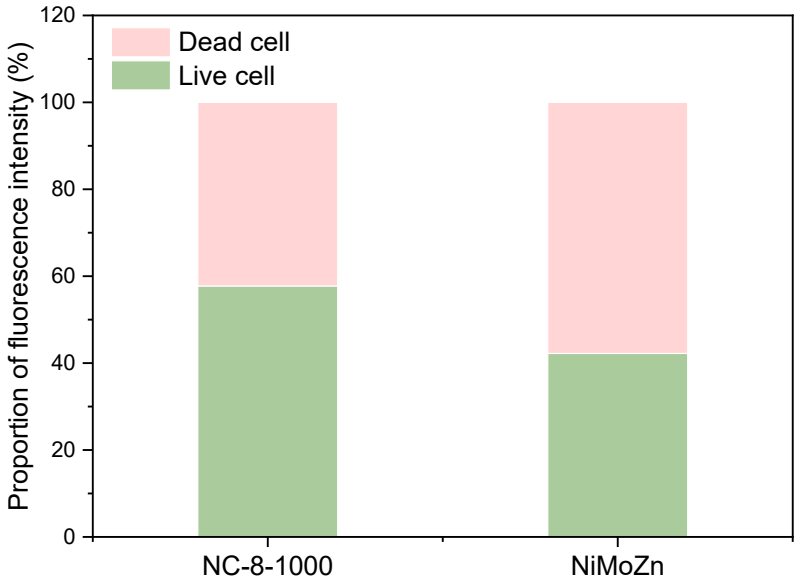

Figure S14 Survival rate of *R. eutropha* H16 on the surface of electrodes loaded NC-8-1000 and NiMoZn. (The survival rates of R. eutropha H16 were calculated by the proportion of fluorescence intensity of dead and live cells in the CLSM images. The fluorescence intensity was analyzed by Image J.)

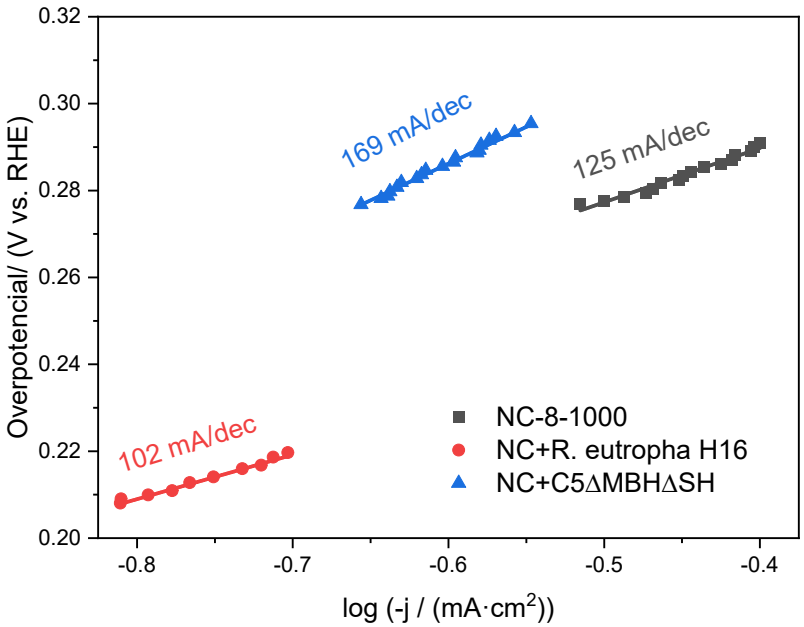

Figure S15 Tafel plot of NC-8-1000, NC-8-1000 loading *R. eutropha H16*, and NC-8-1000 loading C5ΔMBHΔSH.

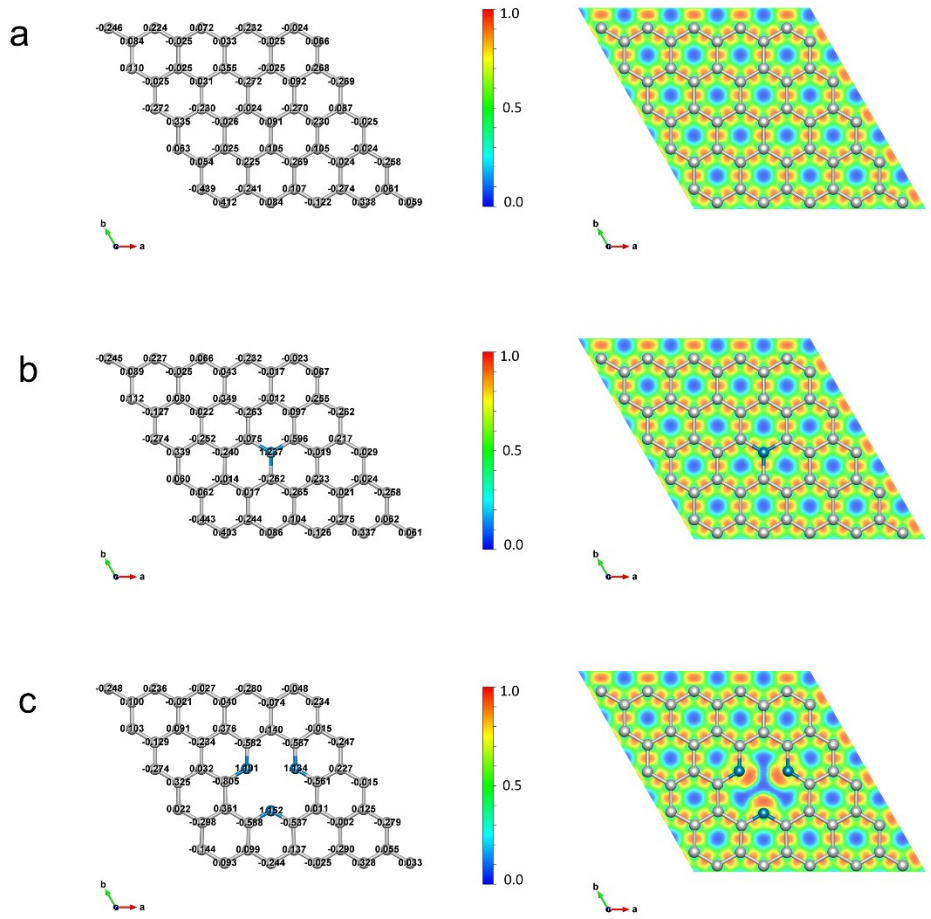

Figure S16 The Bader charge and electron localization function (ELF) calculation results of a) non-nitrogen doping sample, b) graphitic N doping sample, and c) pyridinic N doping sample.

Table S1 Atomic percent (at. %) of C, N, and O of all samples obtained from XPS results.

Atomic %	C	N	O
NC-8-1000	89.85	4.63	5.52
NC-4-1000	91.14	3.66	5.2
NC-1-1000	91.14	3.26	5.61
NC-EDTA-1000	94.12	3.11	2.77
NC-8-900	90.93	5.04	4.03
NC-8-800	87.99	7.54	4.47

Table S2 Atomic concentrations (at. %) of C-C, C-N, C-O, and C=O of all samples in the C 1s binding energy region.

Relative C content / at. %	C-C	C-N	C-O	C=O
NC-8-1000	37.80	35.40	10.12	6.53
NC-4-1000	36.60	40.47	10.05	4.02
NC-1-1000	42.17	35.57	7.88	5.52
NC-EDTA-1000	57.43	21.37	8.07	7.25
NC-8-900	39.20	38.10	9.50	4.14
NC-8-800	38.86	36.72	9.08	3.33

Table S3 Atomic concentrations (at. %) of Pyridinic N, Pyrrolic N, Graphitic N, and Oxidated N of all samples in the N 1s binding energy region.

Relative N content / at. %	Pyridinic N	Pyrrolic N	Graphitic N	Oxidated N
NC-8-1000	0.90	0.59	2.30	0.84
NC-4-1000	0.53	0.40	2.06	0.67
NC-1-1000	0.44	0.34	1.83	0.64
NC-EDTA-1000	0.34	0.31	1.95	0.51
NC-8-900	1.20	0.48	2.45	0.91
NC-8-800	2.53	0.22	3.61	1.18

Table S4 BET results of all samples.

Sample	BET(m^2/g)	Total pore volume (cm^3/g)
NC-8-1000	4765.615	3.068
NC-4-1000	900.269	0.3684
NC-1-1000	792.898	0.3084
NC-EDTA-1000	31.675	0.01147
NC-8-900	1328.347	0.5672
NC-8-800	684.643	0.2695

Table S5 Comparison of the HER performance of all samples in this work.

Sample	Onset potential (mV)	Tafel slope (mA/dec)	U_{-10mA} (mV)
NC-8-1000	275	125	527
NC-4-1000	330	416	731
NC-1-1000	422	583	771
NC-EDTA-1000	679	545	-
NC-8-900	341	127	687
NC-8-800	553	463	-
Pt/C	66	43	124

Table S6 Comparison of the HER performance of NC-8-1000, NiMoZn, and NC-8-1000 after 6 cycles in different electrolytes.

electrolyte	cathode	Onset potential (mV)	Tafel slope (mA/dec)	U_{-10mA} (mV)
1M PBS	NC-8-1000	282	310	672
	NC-8-1000 after 6 cycles	22	76	494
	NiMoZn	19	88	341
72mM MM	NC-8-1000	324	550	-
	NC-8-1000 after 6 cycles	108	226	-
	NiMoZn	75	180	-

Table S7 Analysis of variance for the performance of microbial electrosynthesis in the long-term experiment.

p-value	4.5 mA/cm²	6 mA/cm²	9 mA/cm²
OD_{600}	0.69	0.72	0.73
[Biomass]	0.75	0.80	0.88
[PHB]	0.57	0.74	0.62
PHB/DCW	0.44	0.87	0.95
EE-all/%	0.63	0.22	0.68
EE-PHB/%	0.60	0.61	0.82
EE-biomass/%	0.98	0.59	0.62

One-way analysis of variance (ANOVA) was analyzed ($\alpha = 0.05$) for the performance of microbial electrosynthesis in the long-term experiment. To exclude the influence of different cycle lengths, the last 7 days of each cycle were selected uniformly for calculation. The result of the p-value is listed in Table 5. P>0.05 is "not significant", P<=0.05 is "significant", P<=0.01 is "very significant".

Table S8 Comparison to previous studies of bioelectrochemical systems for CO_2 fixation.

Source	This work	Li. et al.[7]	Schlegel et al.[8]	Li. et al.[9]	Torella et al.[10]	Torella et al.[10]
Organism/strain	*R. eutropha* H16	*R. eutropha* H16	*R. eutropha* H16	*R. eutropha* LH74D	*R. eutropha* H16	*R. eutropha* Re2133-pEG12
Cathode	NC	Ni@N-C	Pt	In	NiMoZn	SS
Anode	Pt	Pt	Pt	Pt	CoP_i	CoP_i
Total Cell Potential, E_{cell} (V)	3.8	~4	~5	~4	2.7	3.0
Reactor volume, V (mL)	150	150	1000	350	35	35
Product 1	PHB	PHB	-	isobutanol	-	isobutanol
Product 1 Amount (mg/L)	538.0	384.3	-	~100	-	216
Product 2	-	-	-	3-methyl-1-butanol	-	-
Product 2 Amount (mg/L)	-	-	-	~50	-	-
Electricity-to-organic Efficiency	7.3%	6.6%	4.8%	2.3%	13%	6.1%
Electricity-to-Biomass Efficiency	4.3%	-	4.8%	1.8%	13%	4.6%
Electricity-to-product Efficiency	3.0%	-	-	0.5%	-	1.5%

Table S9 EDS result of NC-8-1000/CP.

Elt.	Line	Intensity (c/s)	Atomic %	Atomic Ratio	Conc	Units	Error 2-sig	MDL 3-sig
C	Ka	193.28	91.227	13.0869	86.751	wt.%	4.224	2.313
N	Ka	.00	.000	.0000	.000	wt.%	.000	.000
O	Ka	4.97	6.971	1.0000	8.830	wt.%	4.195	5.152
P	Ka	17.45	1.802	.2585	4.419	wt.%	.833	.759
Total			100.000		100.000	wt.%		

Table S10 EDS result of NC-8-1000@CP after 6 cycles.

Elt.	Line	Intensity (c/s)	Atomic %	Atomic Ratio	Conc	Units	Error 2-sig	MDL 3-sig
C	Ka	23.94	30.014	.7366	17.157	wt.%	2.632	2.171
N	Ka	9.80	1.528	.0375	1.768	wt.%	.500	.535
O	Ka	71.60	40.744	1.0000	31.025	wt.%	2.414	1.027
Na	Ka	24.73	5.082	.1247	5.560	wt.%	.828	.660
P	Ka	104.76	11.082	.2720	16.336	wt.%	1.075	.569
K	Ka	30.58	3.376	.0829	6.283	wt.%	.782	.471
Fe	Ka	29.25	7.112	.1745	18.902	wt.%	2.342	1.186
Ni	Ka	2.84	1.063	.0261	2.969	wt.%	1.114	1.671
Total			100.000		100.000	wt.%		

Table S11 Comparison of the HER performance of NC-8-1000, NC-8-1000 loading R. eutropha H16, and NC-8-1000 loading C5ΔMBHΔSH.

Sample	Onset potential (mV)	Tafel slope (mA/dec)	U_{-10mA} (mV)
NC-8-1000	275	125	527
NC-8-1000@ *R. eutropha*	223	102	450
NC-8-1000@C5ΔMBHΔSH	302	169	597

References

1. Reece, S. Y.; Hamel, J. A.; Sung, K.; Jarvi, T. D.; Esswein, A. J.; Pijpers, J. J. H.; Nocera, D. G. Wireless Solar Water Splitting Using Silicon-Based Semiconductors and Earth-Abundant Catalysts. *Science* **2011**, *334* (6056), 645-648.

2. Liu, C.; Colon, B. C.; Ziesack, M.; Silver, P. A.; Nocera, D. G. Water splitting-biosynthetic system with CO2 reduction efficiencies exceeding photosynthesis. *Science* **2016**, *352* (6290), 1210-1213.

3. Kresse, G.; Furthmuller, J. Efficiency of ab-initio total energy calculations for metals and semiconductors using a plane-wave basis set. *Comput. Mater. Sci.* **1996**, *6* (1), 15-50.

4. Blochl, P. E. Projector Augmented-Wave Method. *Phys. Rev. B* **1994**, *50* (24), 17953-17979.

5. Perdew, J. P.; Chevary, J. A.; Vosko, S. H.; Jackson, K. A.; Pederson, M. R.; Singh, D. J.; Fiolhais, C. Atoms, Molecules, Solids, and Surfaces - Applications of the Generalized Gradient Approximation for Exchange and Correlation. *Phys. Rev. B* **1992**, *46* (11), 6671-6687.

6. Grimme, S.; Antony, J.; Ehrlich, S.; Krieg, H. A consistent and accurate ab initio parametrization of density functional dispersion correction (DFT-D) for the 94 elements H-Pu. *J. Chem. Phys.* **2010**, *132* (15).

7. Li, Z. J.; Li, G.; Chen, X. L.; Xia, Z.; Yang, B.; Yao, J. N.; Lei, L. C.; Hou, Y. Water Splitting-Biosynthetic Hybrid System for CO2 Conversion using Nickel Nanoparticles Embedded in N-Doped Carbon Nanotubes. *ChemSusChem* **2018**, *11* (14), 2382-2387.

8. Schuster, E.; Schlegel, H. G. Chemolithotrophic growth of Hydrogenomonas H16 in a chemostat with electrolytic production of oxygen and hydrogen. *Arch. Microbiol.* **1967**, *58* (4), 380-&, DOI: 10.1007/BF00409745.

9. Li, H.; Opgenorth, P. H.; Wernick, D. G.; Rogers, S.; Wu, T. Y.; Higashide, W.; Malati, P.; Huo, Y. X.; Cho, K. M.; Liao, J. C. Integrated Electromicrobial Conversion of CO2 to Higher Alcohols. *Science* **2012**, *335* (6076), 1596-1596.

10. Torella, J. P.; Gagliardi, C. J.; Chen, J. S.; Bediako, D. K.; Colon, B.; Way, J. C.; Silver, P. A.; Nocera, D. G. Efficient solar-to-fuels production from a hybrid microbial-water-splitting catalyst system (vol 112, pg 23337, 2015). *Proc. Natl. Acad. Sci. U. S. A.* **2015**, *112* (12), E1507-E1507.